united nations
educational, scientific
and cultural
organization

international atomic
energy agency

the
abdus salam
international centre for theoretical physics

H4.SMR/1150 - 15

Fifth Workshop on Non-Linear Dynamics
and Earthquake Prediction

4 - 22 October 1999

Distributed, Damage, Faulting, and Friction

A. Agnon

Institute of Earth Sciences,
The Hebrew University,
Jerusalem, Israel

JOURNAL OF GEOPHYSICAL RESEARCH, VOL. 102, NO. B12, PAGES 27,635-27,649, DECEMBER 10, 1997

Distributed damage, faulting, and friction

Vladimir Lyakhovsky
Institute of Earth Sciences, The Hebrew University, Jerusalem

Yehuda Ben-Zion
Department of Earth Sciences, University of Southern California, Los Angeles

Amotz Agnon
Institute of Earth Sciences, The Hebrew University, Jerusalem

Abstract. We present a formulation for mechanical modeling of geological processes in the seismogenic crust using damage rheology. The seismogenic layer is treated as an elastic medium where distributed damage, modifying the elastic stiffness, evolves as a function of the deformation history. The model damage rheology is based on thermodynamic principles and fundamental observations of rock deformation. The theoretical analysis leads to a kinetic equation for damage evolution having two principal coefficients. The first is a criterion for the transition between strength degradation and recovering (healing), and is related to friction. The second is a rate coefficient of damage evolution which can have different values or functional forms for positive (degradation) and negative (healing) evolution. We constrain these coefficients by fitting model predictions to laboratory data, including coefficient of friction in sawcut setting, intact strength in fracture experiments, first yielding in faulting experiments under three-dimensional strain, onset and evolution of acoustic emission, and dynamic instability. The model damage rheology accounts for many realistic features of three-dimensional deformation fields associated with an earthquake cycle. These include aseismic deformation, gradual strength degradation, development of process zones and branching faults around high-damage areas, strain localization, brittle failure, and state dependent friction. Some properties of the model damage rheology (e.g., cyclic stick-slip behavior with possible accompanying creep) are illustrated with simplified analytical results. The developments of the paper provide an internally consistent framework for simulating long histories of crustal deformation, and studying the coupled evolution of regional earthquakes and faults. This is done in a follow up work.

1. Introduction

Rocks exhibit a wide variety of rheological behaviors ranging from viscoelastic deformation to plastic flow and localized faulting. A great challenge of theoretical geodynamic studies is to incorporate multi rheological behavior, including faulting, into models that simulate deformational processes in the upper crust. At the present time, a generally accepted method for describing time-dependent deformational processes in the brittle-elastic parts of the lithosphere is not available. The purpose of this paper and a follow-up work (*V. Lyakhovsky, Y. Ben-Zion, and A. Agnon, manuscript in preparation*; herein after referred to as paper 2) is to develop a useful framework for studies concerned with seismic and aseismic deformations in large domains of space and time. The overall large-scale structure of our model is a layered elastic-viscoelastic half-space incorporating damage rheology. In the present paper we focus on theory and observations relevant to the damage rheology and its coupling with viscous relaxation. In paper 2 we discuss the other components of the model and provide various simulation examples.

Paper number 97JB01896.
0148-0227/97/97JB-01896$09.00

Brittle behavior is often modeled by a rigid elastic-plastic solid that is governed by simple static-kinetic friction or Byerlee's law [*Brace and Kohlstedt*, 1980]. However, such models do not account for details of strength evolution and they thus cannot be used to study important portions of the deformation field, such as nucleation of slip instabilities. The rate- and state-dependent (RS) friction model [e.g., *Dieterich*, 1979, 1981; *Ruina*, 1983] provides a framework that can be used to simulate all important aspects of an earthquake cycle, including stable slip, nucleation of instabilities, rupture propagation, and healing. However, the RS formulation assumes that deformation at all stages occurs on well defined frictional surfaces, and it does not provide a mechanism for understanding distributed deformation. In addition, it is not clear [e.g., *Andrews*, 1989; *Ben-Zion and Rice*, 1995] to what extent the existing RS friction laws are valid for natural conditions involving complex geometry, large values of slip, slip rate, and time, etc.

Various simple conceptual schemes based on a network of blocks and springs [e.g., *Burridge and Knopoff*, 1967; *Carlson and Langer*, 1989] have been used to simulate static, quasi-static, and dynamic sliding processes. *Rice* [1993] and *Ben-Zion* and *Rice* [1993, 1995] criticized the validity of representing a fault in elastic solid with a block-spring array. They simulated slip histories on various types of a two-

dimensional (2-D) strike-slip fault in a 3-D elastic half-space with models incorporating continuum elasticity. *Cowie et al.* [1993], *Sornette et al.* [1994], and *Ward* [1996] simulated the development of fault patterns and regional earthquakes in 2-D elastic solids; we discuss these models in more detail in paper 2. *Lockner and Madden* [1991 a, b] developed a numerical multiple-crack model for the failure process of a brittle solid which simulates growth of microcracks on a regular array of potential crack sites. This and similar numerical models reproduce various common features of fracturing processes, especially those occurring in some fabricated materials, but they cannot explain fault patterns observed in experiments [e.g., *Reches*, 1988] or in the field [e.g., *Segall and Pollard*, 1983]. Fracture distributions in situ and fragmentation of rocks in laboratory samples show fractal-like patterns [e.g., *King*, 1983; *Turcotte*, 1986; *Okubo and Aki*, 1987; *Aviles et al.*, 1987]. Thus fracture network simulations should not depend on specific length scales, such as length scales prescribed in regular arrays.

A rheological model of the faulting process should include subcritical crack growth from very early stages of the loading, material degradation due to increasing crack concentration, macroscopic brittle failure, post failure deformation, and healing. Suitable variables should be defined to characterize the above deformational aspects quantitatively in a framework compatible with continuum mechanics and thermodynamics. Among such approaches are *Robinson*'s [1952] linear cumulative creep damage law, *Hoff*'s [1953] ductile creep rupture theory, *Kachanov*'s [1958, 1986] brittle rupture theory, *Rabotnov*'s [1969, 1988] coupled damage creep theory, and many modifications of these theories. Several researchers (see the review of *Kachanov*, [1994]) proposed models with a scalar damage parameter changing from 0 at an undamaged state to 1 at failure. The scalar damage models fit reasonably well existing experimental results, including culmination of damage in concrete subjected to fatigue loading [*Papa*, 1993] and damage increase in 2024-T3 aluminum alloy under different loading and temperature conditions [*Hansen and Schreyer*, 1994]. In the study of *Hansen and Schreyer* [1994], the scalar isotropic damage model correlates with all measured quantities except the change in the apparent Poisson ratio. For this reason, *Ju* [1990] and *Hansen and Schreyer* [1994] suggested upgrading the damage parameter from a scalar to tensor quantity. Such an anisotropic tensorial damage model contains at least three adjustable parameters which permit correct simulation of the apparent Poisson ratio.

Variations of elastic moduli and Poisson's ratio with extent of damage, under different types of load, can also be described using a nonlinear elastic model with scalar damage provided that it is scaled properly with the ratio of strain invariants. This has been done in the damage model proposed by *Lyakhovsky and Myasnikov* [1984, 1985], *Myasnikov et al.* [1990], and *Lyakhovsky et al.* [1993]. Previous applications of this model to geodynamic problems were given by *Ben-Avraham and Lyakhovsky* [1992], *Lyakhovsky et al.* [1994], and *Agnon and Lyakhovsky* [1995]. The scalar damage model accurately reproduces results from the four point beam test [*Lyakhovsky et al.*, 1997]. Here we provide additional developments of the above model, and constrain the final model parameters by comparisons of theoretical predictions with various laboratory results. In paper 2 we incorporate the damage rheology into a model of a 3-D layered half-space and provide examples of simulated patterns of seismicity and faulting.

2. Distributed Damage in Rocks

We briefly list below some indications of damage in natural rocks and rock samples which form the observational basis for our theoretical damage model for the crust. Pioneering studies of fractures and faults treated the crust as an infinite, perfectly elastic medium [e.g., *Anderson*, 1951]. Subsequent studies accounted for the finite length of faults, and the perturbation to the regional stress field due to the proximity of additional faults [*Chinnery*, 1966 a, b]. Field mapping often shows that the density of faults depends on the scale of the map, so higher resolution increases the number of faults in a given domain [*Scholz*, 1990]. This complexity limits the use of methods that specify the positions of isolated cracks in the deforming region.

Classical fracture mechanics postulates that in a linear elastic solid an isolated crack will propagate at velocities approaching the speed of sound in the medium once a critical stress intensity factor K_c has been reached or exceeded at the crack tip [*Irwin*, 1958]. At lower stress intensity factors the crack remains stable. A more general approach in classical fracture mechanics is to consider the strain energy release rate G during crack extension [e.g., *Freund*, 1990]. Dynamic crack extension occurs when G reaches a critical value G_c.

These fracture mechanics approaches have been used successfully to predict catastrophic crack propagation in metals, ceramics, and glasses. In grainy materials, however, the stress field is highly nonuniform on the grain scale. Stress intensity factors K and strain energy release rates G are calculated macroscopically, neglecting stress concentrations due to grain contacts and energy release due to intergranular sliding. Such materials subjected to long-term loading show significant rates of macroscopic crack extension at values of K and G significantly lower than the critical. This phenomenon is known as subcritical crack growth [*Swanson*, 1984, *Atkinson and Meredith*, 1987; *Cox and Scholz*, 1988].

The investigations of granite fracturing by *Yukutake* [1989], *Lockner et al.* [1991], and *Reches and Lockner* [1994] show that fracturing cannot be described in terms of propagation of a single crack. Several experimental studies revealed that elastic parameters strongly depend on the deformational history (i.e., damage extent), leading to vanishing elastic moduli at large stresses just before failure [*Lockner and Byerlee*, 1980]. While linear elastic fracture mechanics assumes the size of the inelastic zone at the crack tip to be negligibly small, the experiments show that this zone has a significant size.

In most engineering and rock-like materials a slowly propagating crack is preceded by an evolving damage zone distributed around its tip [e.g., *Bazant and Cedolin*, 1991; *Lockner et al.*, 1991]. The distributed damage modifies the elastic coefficients in the medium around the tip and hence controls the macrocrack trajectory and the growth rate [*Huang et al.*, 1991; *Chai*, 1993]. The finite size effect of the fracture process zone is often treated with models which specify a cohesive zone near the crack tip within the plane of the crack [*Dugdale*, 1960; *Barenblatt*, 1962; *Ida*, 1972; *Palmer and Rice*, 1973, *Rubin*, 1995 a, b]. This approach is useful when the crack geometry is well defined, and in contrast to linear elastic fracture mechanics, the cohesion zone models do not contain an unphysical crack tip singularity.

Field observations suggest that the size of the damage zone (or process zone) grows with the size of the fracture, in viola-

tion of the premises of the critical stress intensity factor approach [*Rubin*, 1995 a, b]. This is decisively documented around dikes that form by the injection of magma into fractures [*Delaney et al.*, 1986; *Baer*, 1991; *Weinberger et al.*, 1995; *Hoek*, 1995], and is also compatible with results of *Papageorgiou and Aki* [1983] who inverted seismic strong motion data for earthquake source parameters in the context of their specific barrier model. An early theoretical discussion of this phenomenon is given by *Andrews* [1976].

Andrews and Ben-Zion [1997] showed that earthquake rupture can propagate along an interface separating different elastic media in a wrinkle-like mode associated with little loss of energy to friction. Thus it is energetically favorable for ruptures to be located along the material interface between the gouge and the surrounding rock, rather than within the gouge. In such circumstances the damage zones of successive earthquake ruptures continue to create fresh gouge material, thus adding to the overall thickness of the (damaged) fault zone. This may help to explain field and laboratory correlations [e.g., *Hull*, 1988; *Robertson*, 1983] between gouge thickness and cumulative number of earthquakes (or slip) along the fault.

It is important to consider an additional property of rocks when choosing a rheology for simulations of earthquake cycles. Experimental studies of rock deformation [e.g., *Nishihara*, 1957; *Ambartsumyan*, 1982; *Weinberger et al.*, 1994] reveal a strong dependence of elastic coefficients on the type of loading, which results in abrupt changes of the elastic moduli when the loading reverses from tension to compression. Abrupt changes of elastic properties are commonly observed in grainy materials. For example, the tensile Young modulus of graphite is 20% less than the compressive one [*Jones*, 1977]. Jumps of Young moduli can be 30% for different types of iron, and in concrete the compressive modulus may be up to 3 times larger than the tensile one [*Ambartsumyan*, 1982]. Results of various experiments with Westerly granite, marble, diabase, and weak granite from Kola Peninsula, compiled by *Lyakhovsky* [1990] and *Lyakhovsky et al.* [1993], show high sensitivity of rock elasticity to the type of loading.

It is reasonable to assume that the extent of the latter nonlinearity in the elastic response of rocks depends strongly on the state of damage. Perfectly intact and undamaged rock should not display nonlinear elasticity for small strains. On the other hand, a rock that is highly damaged along a plane can respond to uniaxial extension normal to the damage plane with small elastic stress, whereas it will respond to uniaxial compression in a manner similar to intact rock.

In the following sections we first discuss the thermodynamics of damage growth in elastic solid. Then we construct a phenomenological model that relates damage to the elastic response in an internally consistent manner. Finally, we constrain the obtained model parameters by comparisons of theoretical predictions with experimental results.

3. Model of Medium With Distributed Damage

3.1. General Thermodynamic Formulation

Here we present the construction of a new rheological model accounting for elastic deformation, viscous relaxation, and evolution of damage (material degradation as well as healing). We follow the approach of irreversible thermodynamics [*Onsager*, 1931; *Prigogine*, 1955; *deGroot and Mazur*, 1962], which was successfully applied to kinetics of chemical reactions and phase transitions [e.g., *Fitts*, 1962; *deGroot and Mazur*, 1962] and as a basis for variational methods of continuous media models [e.g., *Sedov*, 1968; *Malvern*, 1969]. Following this framework, *Mosolov and Myasnikov* [1965] first formulated a variational approach to the model of viscoplastic media [see also *Ekland and Temam*, 1976]. *Lyakhovsky and Myasnikov* [1985] first used the balance equations of energy and entropy to establish a thermodynamical foundation for a rheological model of damaged material [*Myasnikov et al.*, 1990; *Lyakhovsky et al.*, 1993]. A similar approach was later used as the basis of other damage models [e.g., *Valanis*, 1990; *Hansen and Schreyer*, 1994].

Many workers in continuum thermodynamics have postulated that the free energy density is a function of various state variables, including "hidden variables" [*Coleman and Gurtin*, 1967; *Lubliner*, 1972] not available for macroscopic observation. In order to simulate a process of fracturing in terms of continuum mechanics, a nondimensional intensive damage variable α is introduced. The variable α can be envisioned as the density of microcracks in a laboratory specimen, or as the density of small faults in a crustal domain. The free energy of a solid, F, is assumed to be given by

$$F = F(T, \varepsilon_{ij}, \alpha), \tag{1}$$

where T and ε_{ij} are the macroscopic temperature and Cauchy tensor of infinitesimal elastic deformation, respectively, and α is a nondimensional damage state variable. The elastic strain tensor ε_{ij} is written as the difference between a current metric tensor g_{ij} and a metric tensor describing the irreversible deformation, g^0_{ij}:

$$\varepsilon_{ij} = g_{ij} - g^0_{ij}. \tag{2}$$

It may be represented through small elastic displacements u_i,

$$\varepsilon_{ij} = \frac{1}{2}\left(\frac{\partial u_i}{\partial x_j} + \frac{\partial u_j}{\partial x_i}\right). \tag{3}$$

The strain rate tensor is given as a temporal derivative of the current metric tensor

$$\dot{\varepsilon}_{ij} = \frac{dg_{ij}}{dt}. \tag{4}$$

The balance equations of the internal energy U and entropy S accounting for irreversible changes of viscous deformation and material damage [e.g., *Malvern*, 1969] have the form

$$\frac{dU}{dt} = \frac{d}{dt}(F + TS) = \frac{1}{\rho}\sigma_{ij}\dot{\varepsilon}_{ij} - \nabla_i J_i, \tag{5}$$

$$\frac{dS}{dt} = -\nabla_i\left(\frac{J_i}{T}\right) + \Gamma, \tag{6}$$

where ρ is mass density. Here J_i is heat flux and Γ is local entropy production. Both J_i and Γ result from dissipative irreversible processes such as internal friction and creation of new surfaces. Substituting (5) into (6) and using an equation for production of free energy [e.g., *Gibbs*, 1961]

$$dF = -SdT + \frac{\partial F}{\partial \varepsilon_{ij}} d\varepsilon_{ij} + \frac{\partial F}{\partial \alpha} d\alpha, \tag{7}$$

and the definition of the Cauchy stress tensor

$$\sigma_{ij} = \rho \frac{\partial F}{\partial \varepsilon_{ij}}. \quad (8)$$

the local entropy production may be represented as

$$\Gamma = -\frac{J_i}{\rho T^2}\nabla_i T + \frac{1}{\rho T}\sigma_{ij}\frac{d\varepsilon_{ij}^0}{dt} - \frac{1}{T}\frac{\partial F}{\partial \alpha}\frac{d\alpha}{dt}. \quad (9a)$$

The first term of equation (9a) describes entropy production by heat conduction, the second term is due to dissipation for a viscous flow, and the third term is related to the damage process. We neglect heat production by radioactive decay and chemical processes. These processes are independent to first order; hence, as is commonly assumed, each term in (9a) must be positive. The part of the entropy production related to the damage process, Γ_α, is

$$\Gamma_\alpha = -\frac{1}{T}\frac{\partial F}{\partial \alpha}\frac{d\alpha}{dt}. \quad (9b)$$

We expand Γ_α as a Taylor series with respect to $d\alpha/dt$ around an equilibrium state $\Gamma_\alpha(\alpha)$ where $d\alpha/dt=0$:

$$\Gamma_\alpha\left(\alpha, \frac{d\alpha}{dt}\right) = \Gamma_0(\alpha) + \Gamma_1(\alpha)\frac{d\alpha}{dt} + \Gamma_2(\alpha)\left(\frac{d\alpha}{dt}\right)^2 \geq 0. \quad (9c)$$

Here Γ_1 and Γ_2 are expansion corfficients. In the case of constant damage the deformational process is reversible and entropy production is zero ($\Gamma_\alpha=0$). This condition implies that $\Gamma_0=0$. The entropy production Γ_α should be nonnegative for any level of damage and direction of its evolution including healing (damage decrease) and destruction (damage increase). That is possible only if the second term of the Taylor series, Γ_1, is identically zero and $\Gamma_2>0$. Thus the quadratic term in (9c) is the dominant term of the Taylor series. Back substitution into (9b) gives

$$\Gamma_2\left(\frac{d\alpha}{dt}\right)^2 = -\frac{1}{T}\frac{\partial F}{\partial \alpha}\frac{d\alpha}{dt}. \quad (9d)$$

From (9b) - (9d) the equation of damage evolution has the form

$$\frac{d\alpha}{dt} = -C\frac{\partial F}{\partial \alpha}. \quad (10)$$

where $C=1/\Gamma_2 T$ is a positive function of the state variables describing the temporal rate of the damage process. We note that (10) describes not only damage increase, but also a process of material recovery associated with healing of microcracks, which is favored by high confining pressure, low shear stress, and especially high temperature.

3.2. Elastic Moduli of a Damaged Material

The elastic properties of a damaged solid should depend on the damage level, and quantification of this has been the subject of much research [e.g. *Kachanov*, 1993]. An undamaged solid with $\alpha=0$ is modeled by an ideal linear elastic material governed by Hook's law. At the other extreme, a material with $\alpha=1$ is densely cracked and loses its stability. Below we describe a nonlinear elastic behavior of damaged material for all values of the damage parameter ($0<\alpha<1$), including strain localization and brittle failure.

Many experimental studies measure nonlinear stress-strain relations for rocks and rock-like materials. For example, *Walsh* [1965] showed that Young's modulus of a cracked elastic solid under uniaxial compression is smaller than the modulus of the same solid without cracks; conversely, crack closure under increasing compressive stress causes a gradual increase in the modulus. Opening and closure of microcracks lead to abrupt changes of elastic properties upon stress reversal from tension to compression [e.g., *Weinberger et al.*, 1994]. Various formulations attempt to model such phenomena. The models of Ambartsumyan-Khachatryan [*Ambartsumyan*, 1982] and *Jones* [1977] assume that the compliance (Poisson's ratio divided by Young's modulus) changes when the associated stress component reverses. *Hansen and Schreyer* [1995] consider opening and closing of microcracks to simulate activation and deactivation of damage in terms of continuum mechanics. For materials with a weak nonlinear response, *Lomakin and Rabotnov* [1978] assumed that the elastic moduli depend only on the type of loading. To evaluate the damage effects, *Lyakhovsky et al.* [1997] derive the macroscopic stress-strain relations for a 3-D elastic solid with noninteracting cracks embedded inside a homogeneous matrix, and test the solution against rock-mechanics experiments. The cracks considered are oriented perpendicular either to the maximum tension axis or maximum compression axis. In the first case they dilate during loading, while in the second they contract. The solution for the elastic energy of such a solid was derived following the self-consistent scheme of *Budiansky and O'Connell* [1976]. Following the formulation discussed by *Lyakhovsky et al.* [1997], the elastic potential is written as

$$U = \frac{1}{\rho}\left(\frac{\lambda}{2}I_1^2 + \mu I_2 - \gamma I_1\sqrt{I_2}\right), \quad (11)$$

where λ and μ are Lame constants, $I_1=\varepsilon_{kk}$ and $I_2=\varepsilon_{ij}\varepsilon_{ij}$ are two independent invariants of the strain tensor ε_{ij}, and γ is an additional elastic modulus (summation notation is assumed). The second order term with the new modulus γ accounts for microcrack opening and closure in a damaged material. The term incorporates nonlinear elasticity even for an infinitesimal strain, and it simulates abrupt change in the elastic properties when the loading reverses from compression to tension. Using (8), the stress tensor is derived from (11) as

$$\sigma_{ij} = \left(\lambda - \gamma\frac{\sqrt{I_2}}{I_1}\right)I_1\delta_{ij} + \left(2\mu - \gamma\frac{I_1}{\sqrt{I_2}}\right)\varepsilon_{ij}. \quad (12)$$

The stress-strain relation (12) can be rewritten to mimic the usual form of Hook's law by introducing effective elastic moduli

$$\lambda^e = \lambda - \frac{\gamma}{\xi}; \quad \mu^e = \mu - \frac{1}{2}\gamma\xi, \quad (13)$$

where the strain invariant ratio $\xi=I_1/\sqrt{I_2}$ characterizes the type of deformation as discussed below.

Lyakhovsky and Myasnikov [1987, 1988] discussed the relation between seismic wave velocity and state of stress for the damage rheology model we use. They found that small amplitude harmonic waves propagate in this model as in a linear anisotropic elastic solid with elastic stiffness tensor depending on the initial state of strain. Three different modes of waves exist, one P wave and two S waves. Thus in spite of its initial isotropic formulation and a scalar damage parameter, the present nonlinear elastic model accounts for a stress-induced anisotropy.

The energy in the form of (11) is used below to describe the elastic behavior of a damaged material with intermediate values of the parameter α ($0<\alpha<1$).

Table 1. Matrix $\partial^2 U/\partial\varepsilon_{ij}\partial\varepsilon_{kl}$

	ε_{11}	ε_{22}	ε_{33}	ε_{12}	ε_{13}	ε_{23}
ε_{11}	$\lambda+2\mu-\gamma\xi$ $+\gamma\xi e_1^2-2\gamma e_1$	$\lambda-\gamma(e_1+e_2)$ $+\gamma\xi e_1e_2$	$\lambda-\gamma(e_1+e_3)$ $+\gamma\xi e_1e_3$	0	0	0
ε_{22}	$\lambda-\gamma(e_1+e_2)$ $+\gamma\xi e_1e_2$	$\lambda+2\mu-\gamma\xi$ $+\gamma\xi e_2^2-2\gamma e_2$	$\lambda-\gamma(e_2+e_3)$ $+\gamma\xi e_2e_3$	0	0	0
ε_{33}	$\lambda-\gamma(e_1+e_3)$ $+\gamma\xi e_1e_3$	$\lambda-\gamma(e_2+e_3)$ $+\gamma\xi e_2e_3$	$\lambda+2\mu-\gamma\xi$ $+\gamma\xi e_3^2-2\gamma e_3$	0	0	0
ε_{12}	0	0	0	$2\mu-\gamma\xi$	0	0
ε_{13}	0	0	0	0	$2\mu-\gamma\xi$	0
ε_{23}	0	0	0	0	0	$2\mu-\gamma\xi$

Here $e_i=\varepsilon_i/\sqrt{I_2}$ is a normalized value of the deformation along principal axes "i".

3.3. Loss of Convexity and Strain Localization

Two different mathematical conditions are appropriate for analyzing material stability. The first is convexity of the elastic energy which provides a unique solution of the static problem [*Ekland and Temam*, 1976]. This criterion was adopted and expanded by R. Hill, T.Y. Thomas, J. Mandel, C. Trusdell, and others [*e.g. Bazant and Cedolin*, 1991]. The second is ellipticity of the elasto dynamic equation [e.g., *Rudnicki and Rice*, 1975]. These two conditions are not always identical, especially for nonlinear elasticity [e.g., *Schreyer and Neilsen*, 1996 a, b]. The first condition is a stronger one, and convexity may be lost prior to the ellipticity. For that reason we start with the first condition for material stability.

The maximum possible value of the damage parameter α for a given strain tensor ε_{ij} is defined by the requirement of convexity of the elastic energy U of (11). This condition implies positivity of all eigenvalues of the matrix $\partial^2U/\partial\varepsilon_{ij}\partial\varepsilon_{kl}$ whose dimension is 6x6 for six independent components of the strain tensor (ε_{11}, ε_{22}, ε_{33}, ε_{12}, ε_{13}, ε_{23}). The matrix components in the coordinate system of the principal axes are given in Table 1. The first eigenvalue is equal to

$$x_1=2\mu-\gamma\xi=2\mu^e\geq 0. \tag{14}$$

This condition implies stability against simple-shear deformation. The second and third eigenvalues satisfy the quadratic equation

$$x^2-(4\mu-3\gamma\xi+3\lambda)x+(2\mu-\gamma\xi)^2+$$
$$+(2\mu-\gamma\xi)(3\lambda-\gamma\xi)+(\lambda\gamma\xi-\gamma^2)(3-\xi^2)=0.$$

The roots of this equation are nonnegative if

$$(2\mu-\gamma\xi)^2+(2\mu-\gamma\xi)(3\lambda-\gamma\xi)+$$
$$+(\lambda\gamma\xi-\gamma^2)(3-\xi^2)\geq 0. \tag{15}$$

If either (14) or (15) is not satisfied, the elastic energy is not a convex function of the strain tensor and the static problem has multiple solutions. It can be shown that conditions (14) and (15) coincide with conditions of positivity of the eigenvalues of the acoustic matrices which correspond to two different polarizations of shear waves. Thus loss of convexity of the elastic energy in the present model also provides the criterion for strain localization used by *Rudnicki and Rice* [1975].

3.4. Kinetics of the Damage Process

Equation (10) provides a general form of damage evolution compatible with thermodynamic principles. Practical use of the equation requires an additional functional relation between the damage parameter α and the three elastic moduli λ, μ, and γ. With the current level of experimental constraints, some simple assumptions should be made. Hence we assume linear dependencies of the elastic moduli λ, μ, and γ on damage:

$$\lambda=\lambda_0+\alpha\lambda_r,$$
$$\mu=\mu_0+\alpha\mu_r, \tag{16}$$
$$\gamma=\alpha\gamma_r,$$

where $\lambda=\lambda_0$, $\mu=\mu_0$, and $\gamma=0$ correspond to initial elastic moduli of the uncracked material. Combining equations (10), (11), and (16) yields an equation of damage evolution

$$\frac{d\alpha}{dt}=-C\rho\left(\frac{\lambda_r}{2}I_1^2+\mu_rI_2-\gamma_rI_1\sqrt{I_2}\right). \tag{17}$$

which may be rewritten in the form

$$\frac{d\alpha}{dt}=-C_dI_2\left(\frac{\lambda_r}{2\gamma_r}\xi^2+\frac{\mu_r}{\gamma_r}-\xi\right). \tag{18}$$

The positive coefficient C_d, given by $C\rho\gamma_r$, describes the rate of damage evolution for a given deformation.

To use equation (18) in a 3-D damage evolution model, we employ two additional constraints. The first is that there exists a critical strain invariant ratio ξ_0 which corresponds to a neutral state between healing and degradation of the material. As will be shown in a later section, this is a generalization of friction, which is a widely observed constitutive behavior in rocks and other brittle materials. High shear strain relative to

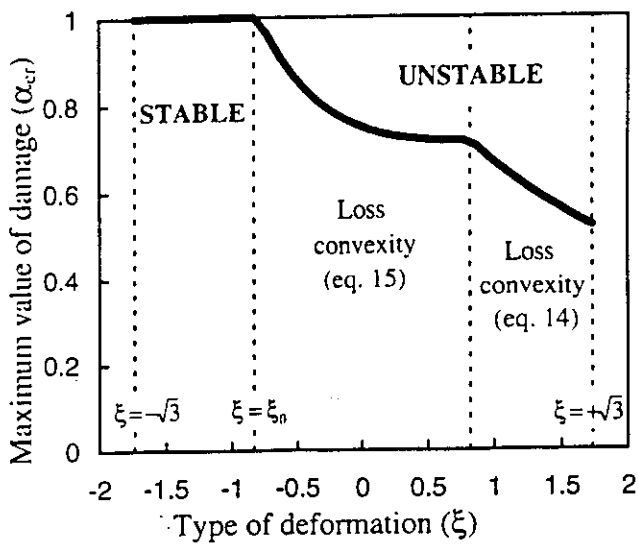

Figure 1. Thick line gives the maximum value (α_{cr}) of the damage parameter α as a function of strain invariant ratio ξ. The range $-\sqrt{3}<\xi<\xi_0$ corresponds to stable behavior with healing. For $\xi>\xi_0$ there is material degradation leading to loss of stability according to equation (14) or (15).

compaction ($0>\xi>\xi_0$) or extension ($\xi>0>\xi_0$) leads to degradation, while high compaction with absence of or low shear component ($\xi<\xi_0$) leads to healing of the material. The coefficient ξ_0 may be estimated from the onset of damage-induced instability or first yielding in rock mechanics experiments. An intuitive possibility for the second constraint, discussed by *Lyakhovsky* [1988] for a similar model, is that of a constant bulk modulus ($\lambda^e+2/3\mu^e$) under isotropic compaction ($\xi=-\sqrt{3}$). However, back substitution to (18) gives with this assumption a zero rate of healing for $\xi=-\sqrt{3}$. This is a significant shortcoming for a model expected to describe earthquake cycles containing both degradation and healing. *Agnon and Lyakhovsky* [1995] slightly changed this assumption and chose only the modulus λ to be constant. Under their condition (16) has the following form

$$\lambda = \lambda_0 = \text{const}; \quad \mu = \mu_0 + \alpha\xi_0\gamma_r; \quad \gamma = \alpha\gamma_r \,. \tag{19}$$

where γ_r is calculated from the conditions (14) and (15) of convexity loss for the maximum value of the damage parameter ($\alpha=1$), when the strain invariant ratio is $\xi=\xi_0$. Figure 1 shows the dependence of the critical damage on the strain invariant ratio for $\lambda_0=\mu_0$. In this case, condition (15) is realized first for $\xi\geq\xi_0$ and prescribes the scale γ_r.

With the assumptions (19), equation (18) is rewritten in a simple form containing only two unknown model parameters

$$\frac{d\alpha}{dt} = C_d I_2(\xi - \xi_0) \,. \tag{20}$$

The two model parameters ξ_0 and C_d are assumed in our model to be material properties. As will be discussed in a subsequent section, the parameters may be constrained by results of rock mechanics experiments. Comparing our model predictions with laboratory data of rate and state-dependent friction, representing average properties of sliding surfaces, we find that in such a context the coefficient C_d does depend on damage. Accordingly, we adopt in that section different rate coefficients (equation 42) for material degradation and healing.

4. General Properties of Damaged Material

In this section, three general properties of the model are analyzed using analytical solutions. The first solution for a 1-D extension problem illustrates strain and damage localization in a previously weakened zone. The second, 2-D case, suggests that there is no stress singularity around a fully destroyed zone. The last example shows that the interaction between the damage evolution and viscous relaxation results in stick-slip shear motion.

4.1. One-Dimensional Deformation

For a uniaxial strain, assuming a linear dependence of Young modulus on damage, $E=E_0[1-\alpha]$, reduces equation (20) to

$$\frac{d\alpha}{dt} = A\left(\frac{\partial u}{\partial x}\right)^2 . \tag{21}$$

where u is displacement depending only on the x coordinate, and A is a coefficient which depends on the type of loading. Since in the 1-D case the strain invariant ratio is $\xi=\pm1$, A is one of two constants: $C_d(1-\xi_0)$ for tension or $C_d(-1-\xi_0)$ for compression. Positive and negative values of A correspond to fracturing and healing, respectively. For the 1-D case we consider only a fracturing process.

We investigate the damage evolution of a body with unit length and fixed displacements at the boundaries, $u(0)=0$ and $u(1)=u_0$, in a one-dimensional deformation. These boundary conditions give the body stress

$$\sigma = u_0\left[\int_0^1 \frac{dx}{E_0(1-\alpha)}\right]^{-1} , \tag{22}$$

and the strain is given by

$$\frac{\partial u}{\partial x} = u_0\left[E_0\cdot(1-\alpha)\int_0^1 \frac{dx}{E_0\cdot(1-\alpha)}\right]^{-1} . \tag{23}$$

Substitution of (23) into (21) results in an equation of damage evolution for the investigated body,

$$\frac{d\alpha}{dt} = Au_0^2\left[(1-\alpha)\int_0^1 \frac{dx}{1-\alpha}\right]^{-2} . \tag{24}$$

For a uniform initial condition ($\alpha|_{t=0}=\text{const}$), equation (24) has the solution $\alpha(t)=At$, leading to a complete destruction of the body with finite time. For a nonuniform initial condition ($\alpha|_{t=0}\neq\text{const}$), the solution of (24) may be written in the form

$$\alpha(x,t) = 1 - \frac{1}{E_0}\sqrt[3]{[E_0(1-\alpha(x,0))]^3 - f(t)} \,, \tag{25}$$

where $f(t)$ depends on $\alpha(x,0)$. Equation (25) implies that the deformation localizes at a point x_0 which is the maximum of the initial damage distribution. To see that, assume that at some time t' the elastic modulus in the interval $[x_0-c, x_0+c]$ may be approximated by a parabola

$$E(x,t') = E_0(1-\alpha(x,t')) = a^2(x-x_0)^2 + b^2 . \tag{26}$$

Substitution of (25) and the parabolic approximation (26) of the modulus into (23) yields a corresponding approximation of the strain distribution in the vicinity of the point x_0.

$$\frac{\partial u}{\partial x} \approx \frac{abu_0}{2\arctan(ac/b)\left[a^2(x-x_0)^2+b^2\right]} - \frac{abu_0}{\pi\left[a^2(x-x_0)^2+b^2\right]} \to \delta(x-x_0). \tag{27}$$

Equation (27) shows that the deformation localizes in the vicinity of the point x_0, where the initial damage distribution was maximum, during a process where the damage at x_0 approaches unity or elastic modulus goes to zero ($b/au_0 \to 0$).

Now consider the elastic energy transfer from the relaxing part of the body to surface energy of the localized damaged zone. We assume that $\alpha(x,0)=\alpha_2$ over a small interval of length L, and $\alpha(x,0)=\alpha_1$ ($<\alpha_2$) elsewhere. In this case, the solution of equation (21) may be represented as $\alpha(x,t)=\alpha_2(t)$ at points initially belonging to the interval L, and $\alpha(x,t)=\alpha_1(t)$ elsewhere. On the basis of (24), the two time-dependent functions α_1 and α_2 satisfy

$$\frac{d\alpha_1}{dt} = Au_0^2\left[\frac{1-\alpha_2}{(1-L)(1-\alpha_2)+L(1-\alpha_1)}\right]^2, \qquad \frac{d\alpha_2}{dt} = Au_0^2\left[\frac{1-\alpha_1}{(1-L)(1-\alpha_2)+L(1-\alpha_1)}\right]^2. \tag{28}$$

For small α_1 and α_2 and with $L \to 0$, equations (28) dictate at the initial stage of the damage evolution an increase of α_2 with a rate greater than the rate of increase of α_1. Thus the ratio α_2/α_1 increases with time. This is in line with the previous result on strain localization for a continuous distribution. The damage process localizes in the interval where the initial damage is high. At the final stage of the evolution, with $\alpha_2 \to 1$, equations (28) have the solutions

$$\alpha_1 = \text{const}; \qquad \frac{d\alpha_2}{dt} = \frac{Au_0^2}{L^2(1-\alpha_1)^2}.$$

The damage process continues only in the small L interval, where $\alpha(t)$ achieves a unit value at finite time and macroscopic failure of the body occurs. The energy transferred into the high damage region, $G=\int\sigma v dt$, can be written from the previous results as

$$G = L(1-L)u_0^2E_0(1-\alpha_1)^2 \times \int \frac{(1-\alpha_2)\dot{\alpha}_2}{\left[(1-\alpha_1)L+(1-\alpha_2)(1-L)\right]^3}dt. \tag{29}$$

Integrating (29) from a time when $\alpha_2 = \bar{\alpha}_2$ to the time of destruction when $\alpha_2=1$, the energy flux G remains finite and is given by

$$G = \frac{E_0u_0^2(1-\alpha_1)}{2(1-L)} - L\frac{E_0u_0^2(1-L)\left[(1-\alpha_1)L+2(1-\bar{\alpha}_2)\right]}{2\left[(1-\alpha_1)L+(1-\bar{\alpha}_2)(1-L)\right]^2}. \tag{30}$$

For the limiting situation $L \to 0$ the energy transfer is $G_{tr}=1/2E_0u_0^2(1-\alpha_1)$. In this case it is seen that all the elastic energy of the relaxed part of the body is transferred to surface energy of the damaged zone. If the rate of the damage process (given by the constant A) is sufficiently large, and/or the length of the initially damaged part is sufficiently small, the rate of the deformational process will increase and part of G_0 will become kinetic and radiate acoustic waves. In this case, only a portion of the initial elastic energy is converted to a surface energy.

4.2. Two-Dimensional Stress Concentration

Extrapolating the results of the previous example to a 2-D case, one may expect strain and damage localization in a small region which leads to stress concentration similar to linear elasticity. However, continuous damage evolution until total destruction eliminates the classical stress singularity. To illustrate that, we analyze stress amplification around a circular hole in a 2-D plate subjected to remote isotropic extension. In a cylindrical coordinate system, only the radial component $\omega_1=\omega(r)$ of the elastic displacements is nonzero, and the stress tensor is given by

$$\sigma_{rr} = \lambda\left(\frac{d\omega}{dr}+\frac{\omega}{r}\right)+2\mu\frac{d\omega}{dr}, \qquad \sigma_{\theta\theta} = \lambda\left(\frac{d\omega}{dr}+\frac{\omega}{r}\right)+2\mu\frac{\omega}{r}, \qquad \sigma_{r\theta} = 0. \tag{31}$$

Using (31) in the equation of equilibrium for the linear elastic material gives a general solution in the form

$$\omega(r) = Ar + \frac{B}{r}. \tag{32}$$

From (32) the stress distribution around a circular hole with radius R in the linear elastic plate subjected to remote extension p is

$$\sigma_{rr} = p\left(1-\frac{R^2}{r^2}\right), \qquad \sigma_{\theta\theta} = p\left(1+\frac{R^2}{r^2}\right). \tag{33}$$

The solution has a stress amplification at the boundary ($\sigma_{\theta\theta}|_{r=R} = 2p$) and a $1/r^2$ decay. As a result of this amplification, the damage process starts at the edge of the hole and it is localized in a thin boundary layer having high gradients of damage and elastic moduli variations. The elastic displacement $\omega(r)$ has a corresponding high gradient near r=R, and in that region the term $d\omega/dr$ is dominant in relations (31) for the stress tensor. Neglecting the term ω/r for a finite radius R of the hole, and using the boundary condition $\sigma_{rr} = 0$, give instead of (32) the condition ω=const ($d\omega/dr=0$) at the boundary. If the damage at the boundary reaches its critical value, the tangential stress component there becomes zero in addition to the radial component. Stress components around the circular hole in a damaged material remain finite even for infinitely small radius of curvature. Instead of singular-like stress distribution, the model predicts an evolving high gradient damage or process zone. The geometry of the process zone and the rate of damage evolution are controlling factors for both the crack trajectory and the rate of crack growth in most engineering materials [*Chudnovsky et al.*, 1990; *Huang et al.*, 1991].

4.3. Stick-Slip Motion

The previous cases neglect viscous stress relaxation and deal only with elastic behavior of damaged material. Here we analyze in one dimension the behavior of a viscoelastic dam-

age material subjected to a constant shear strain rate. For simplicity, the viscosity of the material η is assumed constant. The constitutive relation for a Maxwell viscoelastic body is

$$e = \frac{d}{dt}\left(\frac{\tau}{2\mu}\right) + \frac{\tau}{2\eta}, \tag{34}$$

where τ is shear stress and e is total strain rate (equation 4). As discussed above, the shear modulus μ (equation 19) is assumed to be a linear function of the damage parameter. Thus the equation of damage evolution (20) may be represented by

$$\frac{d\mu}{dt} = C_d \xi_0 \gamma_r \left[\left(\frac{\tau}{2\mu}\right)^2 - \varepsilon_{cr}^2\right]. \tag{35}$$

where ε_{cr} is a critical strain corresponding to the onset of material degradation. For a given dilation I_1, ε_{cr} corresponds to a certain ξ_0. When the deformation is larger than ε_{cr} the damage increases, and when it is lower the damage decreases. Thus the elastic modulus changes together with the damage between zero (loss of convexity and stress drop) and its maximum value. Within these limits the system of equations (34) and (35) has a singular saddle point corresponding to the unstable equilibrium solution

$$\tau = 2\eta e; \quad \mu = \frac{\eta e}{\varepsilon_{cr}}. \tag{36}$$

The two coupled nonlinear equations (34) and (35) describe the temporal variations of shear stress and shear modulus in a damage material subjected to a constant rate of shear strain. The Maxwell relaxation time is $t_v = \eta/\mu$, while a characteristic time scale of the damage process is of the order of $t_d = \mu_v/C_d\gamma_r(\varepsilon^2 - \varepsilon_{cr}^2)$, or $t_d = \mu_v/C_d\gamma_r\xi_0 I_2(\xi - \xi_0)$ for a 3-D problem. The ratio t_v/t_d controls the style of evolution of the mechanical system. A small t_v/t_d implies that the shear stress τ can increase for a given strain rate without significant change in the elastic modulus of the material. If this stress causes the elastic strain to be less than critical, then stable creep is realized. A higher level of the applied strain rate results in elastic strain larger than the critical, which leads to material degradation and stress drop. No significant material healing is expected after stress drop, and the applied constant strain rate does not produce significant consequent stress.

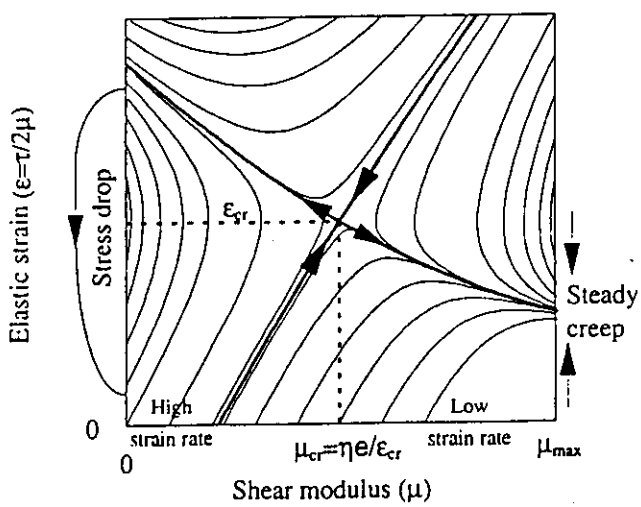

Figure 2. Phase plane with evolution of viscoelastic damage material subjected to a constant strain rate.

The material evolution displays another style if the ratio t_v/t_d is of the order of 1 (Figure 2). Relatively low applied strain rates ($e \sim \mu\varepsilon_{cr}/\eta$) correspond to a set of trajectories tending to stable creep. The shear modulus is increased up to its maximum value and the shear stress approaches the value $\tau = 2\eta e$. Higher strain rates ($e \gg \mu\varepsilon_{cr}/\eta$) also produce material healing at the initial stage of evolution, but the critical elastic strain ε_{cr} is achieved before the shear modulus obtains the value $\mu_{cr} = \eta e/\varepsilon_{cr}$ (horizontal dashed line in Fig. 2). At this point the damage evolution reverses its direction, and a degradation stage begins, leading to a stress drop. The dynamic stress drop, which is not analyzed here, quickly reduces the elastic strain to some low value, keeping zero shear modulus. There is a locus of trajectories that starts from the line $\mu = 0$ and shows significant material recovering together with increase of elastic strain. When the shear stress is large enough, the damage evolution reverses direction again, and a new degradation stage begins, leading to the next stress drop. If the strain rate is so high that the value μ_{cr} is larger than the maximum shear modulus of the material with zero damage, the steady creep can not be realized, and only stick-slip behavior occurs. This process forms a repeating limit cycle which physically corresponds to stick-slip shear motion of the viscoelastic damage material.

5. Estimation of Model Parameters

Savage et al. [1996] draw a connection between macroscopic friction measured on saw-cut specimens and internal friction that characterizes shear fracture of intact rock. They write the strength of an intact rock as the sum over the plane of the incipient fault of both friction on closed microcracks and strength of the remaining grains. The approach taken here extends that connection. We focus our attention on confining pressures sufficient for closure of microcracks, so stress concentration may arise only once the shear stress meets the frictional criterion. Then favorably oriented cracks slide and load their tips giving rise to damage increase (equation 20). The difference between the frictional strength of prefaulted surfaces and the strength of the intact rock is given by the excess stress that is needed to increase the damage from its initial value to critical. That stress difference is rate dependent; since it can be calculated readily from the model, it constrains the rate coefficient C_d. In the limit that the strain remains near-critical for damage growth ($\xi - \xi_0 \to 0$), the time for fracture is infinite, but the strength is friction-like. In this case a smooth surface will evolve along which the damage will approach the critical level ($\alpha \to 1$). These features are explored below analytically, and illustrated by numerical examples. Our main concern here is to estimate the model parameters ξ_0 and C_d which govern the style of damage evolution. The parameter ξ_0 may be estimated from different types of rock mechanics experiments; the parameter C_d is less well constrained.

5.1. Friction and the Onset of Damage

One of the best studied rock property is the friction angle. We relate the critical strain invariant ratio ξ_0 to the friction angle φ by considering the critical shear stress for Mohr-Coulomb sliding:

$$\tau = \tan(\varphi)\sigma_n,$$

where σ_n is normal stress. Consider a saw-cut interface between two intact blocks in a friction experiment carried out

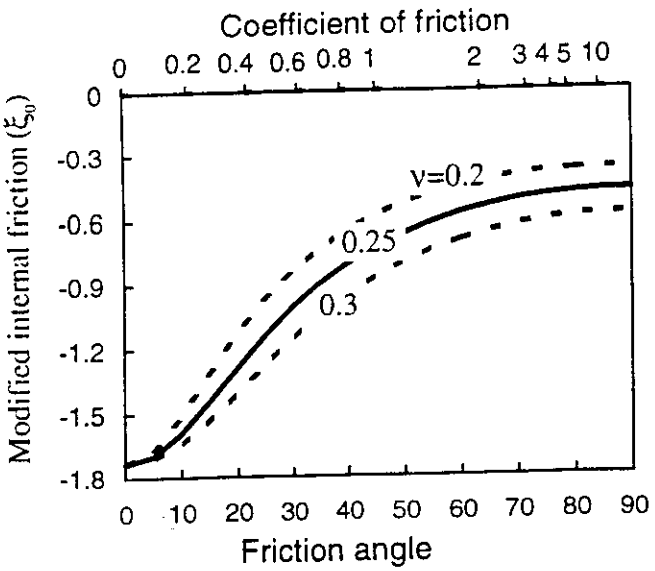

Figure 3. Modified internal friction ξ_0 as a function of friction for different Poisson ratios ν=0.2, 0.25, and 0.3.

under confining pressure. Except for the interface (and perhaps thin adjacent boundary layers), the sample has negligible damage. Stresses are transmitted elastically to the interface, and the corresponding strain can be calculated using Hook's law and conditions of triaxial compression ($\varepsilon_{11}=\varepsilon_{22}>\varepsilon_{33}<0$). The condition for fault slip is then [*Agnon and Lyakhovsky*, 1995]

$$\xi_0 = \frac{-\sqrt{3}}{\sqrt{2q^2(\lambda_e/\mu_e + 2/3)^2 + 1}}, \qquad (37)$$

where

$$q = \frac{\sin(\varphi)}{1-\sin(\varphi)/3}.$$

Physically (37) means that the model parameter ξ_0 is some modification of the internal friction. Figure 3 shows the dependency of the modified internal friction (ξ_0) on the friction for three values of λ_e/μ_e corresponding to values of Poisson ratio 0.2, 0.25, and 0.3. Thus for Westerly granite with friction angle φ~30° [*Byerlee*, 1967], equation (37) gives ξ_0~−0.8. The result varies little for different rocks with Poisson ratio values between 0.2 and 0.3.

5.2. Three-Dimensional Faulting Experiments

The modified internal friction ξ_0 may also be estimated using results of faulting experiments under 3-D strain fields given by *Reches* [1983]. Figure 4 displays empirical relationships between the first and second stress invariants for the first yielding in those experiments. The data appear to be well approximated by the relation

$$J_2 = rJ_1^2. \qquad (38)$$

Following the notation of *Reches* [1983], the stress invariants are $J_1=\sigma_1+\sigma_2+\sigma_3$, $J_2=\sigma_1\sigma_2+\sigma_1\sigma_3+\sigma_2\sigma_3$. Most of the experimental points for different rock types can be fitted by equation (38) with the empirical coefficient r=0.20-0.27. Assuming that the initial rock samples have negligible levels of damage until the first yielding (i.e., that they behave as linear Hookean solids with elastic moduli λ_0, μ_0) and using Hook's law, the modified internal friction ξ_{y1} associated with initiation of the damage process is given from the stress (equation 38) as

$$\xi_{y0} = \frac{-\sqrt{2}}{\sqrt{3(\lambda_0/\mu_0)^2 + 4\lambda_0/\mu_0 + 2 - r(3\lambda_0/\mu_0 + 2)^2}}. \qquad (39)$$

Taking the Poisson's ratio of the rocks close to 0.25 ($\lambda_0=\mu_0$), the corresponding range of variation of ξ_{y0} is found from (39) to be between −0.7 and −1. Our previous estimate based on Byerlee's law for axial symmetric compression experiments (37) falls within this range.

5.3. Onset of Acoustic Emission

The emission of acoustic signals during compressive failure experiments begins at the onset of dilatancy, and this activity accelerates in proportion to the rate of dilatancy which is often observed together with localization of deformation [*Scholz*, 1990 and references therein]. Figure 5a shows observed acoustic emission (AE) data of *Sammonds et al.* [1992], obtained during a deformational experiment on Darley Dale sandstone with a nominal strain rate of 10^{-5} s^{-1} and confining pressure of 50 MPa. After a roughly linear elastic loading in the first 2500 s (axial stress up to 220 MPa) there is a steep rise in AE associated with first yielding and onset of cracking. Material degradation then leads to a second yielding, involving dynamic instability and abrupt stress drop at 3700 s (peak stress of about 290-300 MPa). The observed first and second yielding points can be used to estimate the model parameters ξ_0 and C_d. In our framework, the damage of the sample, initially assumed equal to zero (α=0), starts to increase rapidly at the first yielding when the deformation exceeds the critical value ξ_{y0}. Calculated damage evolution, obtained from equation (20), is similar to the experimental rise in AE rate (Figure 5b). The calculations give loss of convexity, or dynamic stress drop, within a finite period of time and allow us to estimate the second model parameter C_d. We obtain a good fit to the

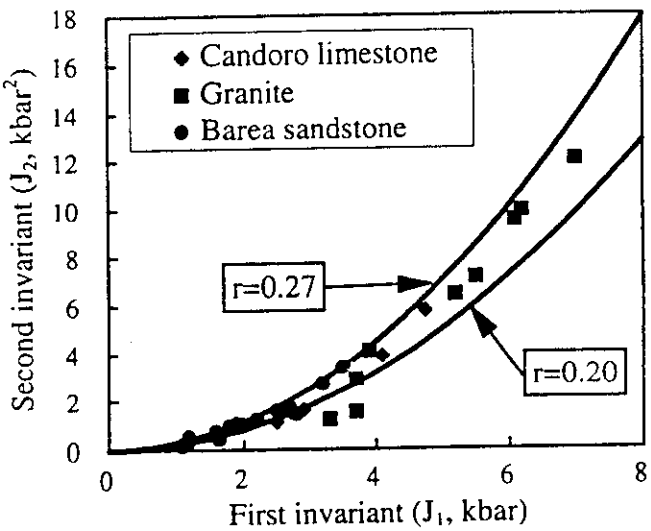

Figure 4. Experimental relations between first ($J_1=\sigma_1+\sigma_2+\sigma_3$) and second ($J_1=\sigma_1\sigma_2+\sigma_1\sigma_3+\sigma_2\sigma_3$) stress invariants at the first yielding under 3-D stress field for different types of rocks [after *Reches*, 1983], and their approximation by equation (38).

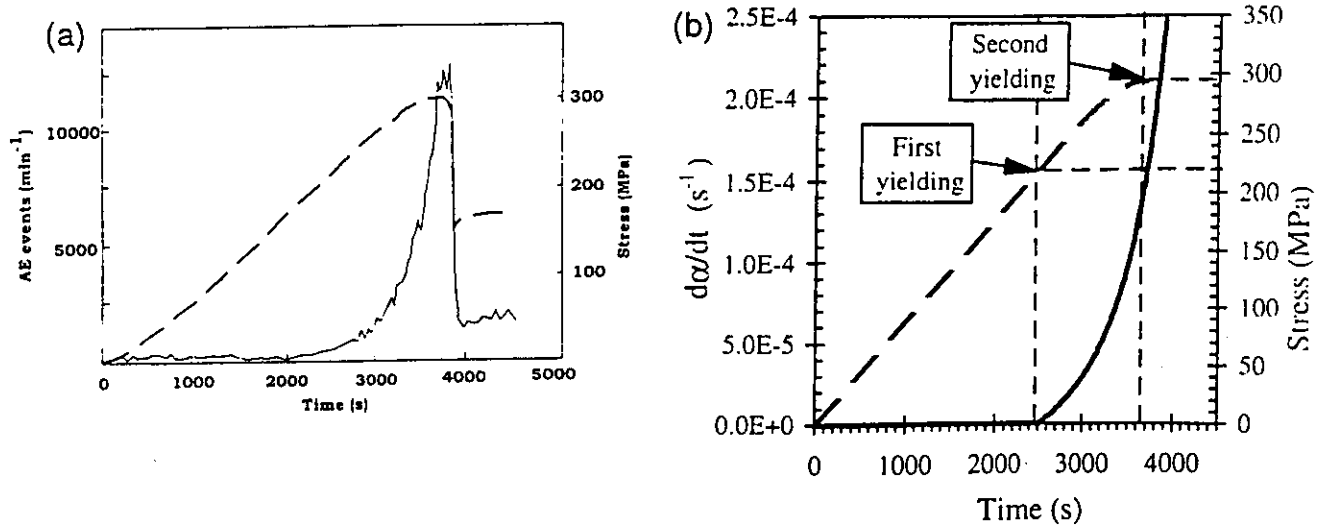

Figure 5. (a) Observed acoustic emission (solid line) and axial stress (dashed line) during deformational experiment on Darley Dale sandstone with a nominal strain rate of 10^{-5} s^{-1} and confining pressure of 50 MPa (Modified with permission from *Nature* [*Sammonds et al.*, 1992]; copyright Macmillan Magazines Limited). (b) Calculated damage evolution (dα/dt - solid line) and axial stress (dashed line) by the damage rheology model with ξ_0=–0.75 and C_d=0.5 s^{-1}.

experimental results of *Sammonds et al.* [1992] with ξ_0=–0.75 and C_d=0.5 s^{-1}. The value of the modified internal friction ξ_0 is again in good agreement with the previous estimates.

5.4. Intact Strength

Most experiments on fracture or intact strength of rocks do not record AE and the first yielding is not defined. Only the second yielding is reported. However, these data also can be used to estimate C_d if the strain rate during the loading is reported and the friction angle is given by the angle of saw-cut samples. Figure 6 shows the results of saw-cut Westerly granite samples after *Stesky et al.* [1974], which are in a good agreement with *Byerlee*'s [1967] friction law for Westerly granite

$$\tau = 0.5 + 0.6\sigma_n \quad \text{(kbar)}.$$

Using the previous estimate (ξ_0=–0.8) for Westerly granite based on the Byerlee friction law, damage evolution is simulated for strain rate of $2.7\cdot10^{-5}$ s^{-1} [*Stesky et al.*, 1974] and different values of C_d=1, 3, and 5 s^{-1}. Three lines shown in Figure 6 represent maximum differential stress (stress envelopes) versus confining pressure simulated for the three different C_d. The curve for C_d=3 s^{-1} fits well the experimental data of *Stesky et al.* [1974] and gives another estimate of the damage rate constant.

It appears that the parameter ξ_0 is well constrained and varies little with different types of rocks and loading conditions. The values of the damage rate constant C_d vary by an order of magnitude based on a limited range of experiments with a similar strain rate of about 10^{-5} s^{-1}. Thus additional constraints for C_d with different strain rates are needed. Some of those may come from fitting simulated seismicity patterns of the type discussed in paper 2.

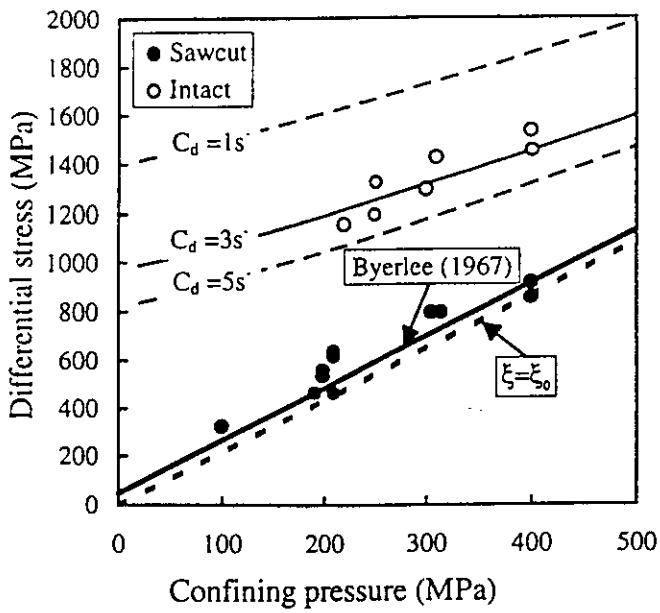

Figure 6. Frictional stress for sawcut series (solid circles) and intact series (open circles) for Westerly granite [after *Stesky et al.*, 1974]. The heavy solid line shows the friction law of *Byerlee* [1967]. The heavy dashed line gives the yielding stress for the modified internal friction ξ_0=–0.8. Thin solid and dashed lines give the simulated yielding stress for C_d=1, 3, 5 s^{-1}.

6. Model Implications

6.1. Necking of Thin Plate

The large-scale extension of thin sheets may, under certain conditions, generate further instabilities by the formation of fault zones or local necks. First we provide an expression for the direction of the neck trace for plastic material. Expressions for a perfectly plastic material were given by *Storen and Rice* [1975] and were used by *Agnon and Eidelman* [1991] for analysis of continental rifts. To maintain a constant length and rigid blocks, the neck must form along horizontal directions of zero extension, or velocity characteristics, symmetrical about

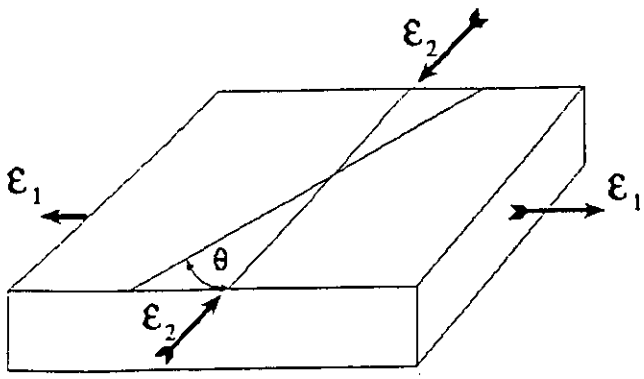

Figure 7. Direction of neck trace in a thin plate with respect to the axis of maximum compression.

the principal incremental strain axes. For incompressible plastic plates, the direction θ between the neck and the axis of maximum compression (Figure 7) is defined by the ratio ρ between the rate of shortening ε_1 and extension ε_2

$$\tan^2(\theta) = \rho = -\frac{\varepsilon_1}{\varepsilon_2}.$$

The orientations of preferred faults in a brittle material were determined by *Reches* [1983] numerically and analytically for different cases. For $\rho \le 0$ the orientation of a fault plane with respect to the coordinate system of the principal strain axes is given from equation (27) of *Reches* [1983]

$$S_1 = \frac{\sqrt{2}}{2}(1+\sin(\varphi))^{1/2},$$

$$S_2 = \frac{\sqrt{2}}{2}|\rho|^{1/2}(1-\sin(\varphi))^{1/2},$$

where S_1 and S_2 are slip directions and φ is a friction angle. The ratio S_1 to S_2 gives the angle θ between the fault plane and axis of maximum compression as

$$\left(\frac{S_1}{S_2}\right)^2 = \tan^2(\theta) = |\rho|\frac{1-\sin(\varphi)}{1+\sin(\varphi)}. \qquad (40)$$

Frictional sliding is characterized by ρ=1, and the angle between a fault trace and the axis of maximum compression can be expressed through the Coulomb criterion as $\theta = \pm(45° - \varphi/2)$. Simple calculations show that equation (40) reproduces exactly this angle for ρ=1.

Figure 8a shows θ for a perfectly plastic plate and a brittle plate with friction angle φ =30°, 40°, 50° (equation 40). Also shown are results of numerical simulations with the present model of damage evolution for a material with the modified internal friction $\xi_0 = -0.8$. This corresponds to a friction angle φ =40° for Poisson ratio ν=0.25 (see Figure 3). Each numerical calculation starts from random initial damage distribution. With time, the damage increases and forms localized zones of very high damage (Figure 8b) with orientation depending on the parameter ρ. The values based on the numerical simulations fit well the prediction of the fault plane orientation in brittle material. These results, and additional simulations discussed in paper 2, illustrate that our damage rheology model is suitable for the study of the evolution of fault branching and other structural irregularities.

6.2. State Dependent Friction and Nonlinear Healing

Following and confirming the pioneering experiments of *Rabinovicz* [1965] on metals, studies of rock friction provide evidence that the static friction increases slowly with the duration of stationary contact [*Dieterich*, 1972]. *Dieterich*

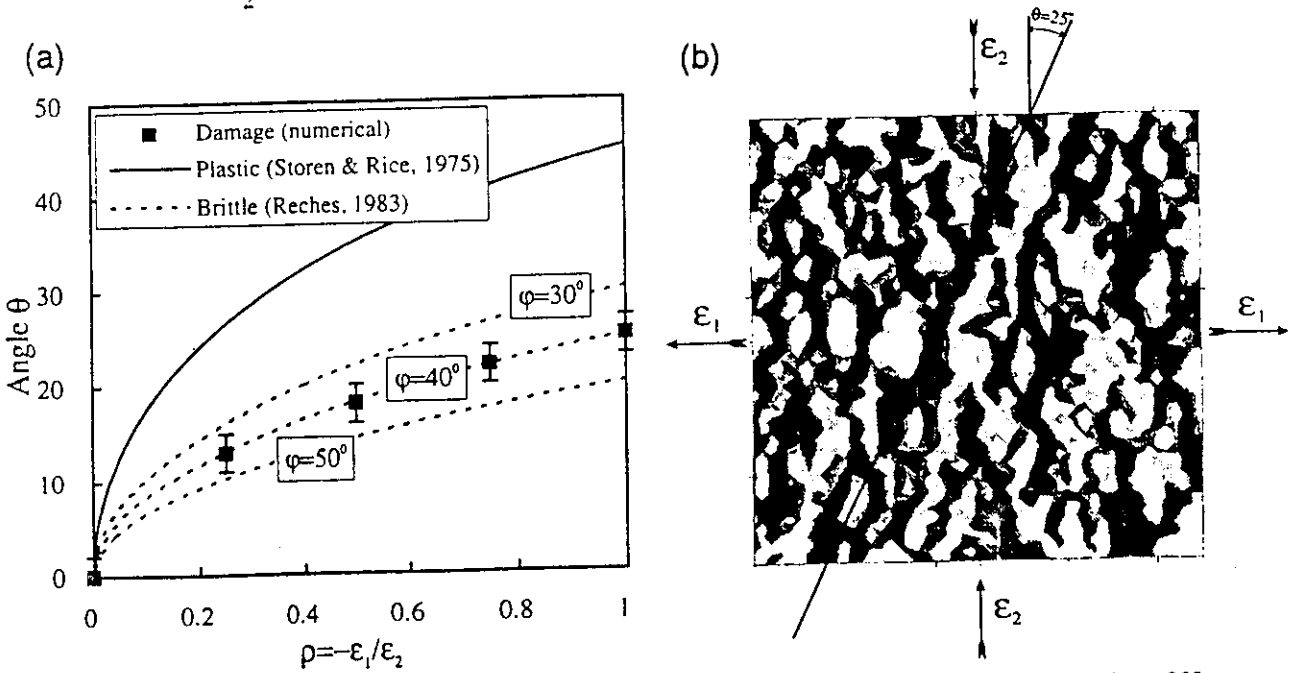

Figure 8. (a) Fault zone orientation in plastic material (heavy line), brittle material with friction angle φ=30°, 40°, and 50° (dashed lines), and model of damage evolution of a material with the modified internal friction $\xi_0 = -0.8$ (squares with vertical bars). The assumed ξ_0 corresponds to the friction angle φ =40° for Poisson ratio ν=0.25 (see Figure 3). (b) Numerical simulation of localized high damage zones in a thin plate under 2-D loading with $\rho = -\varepsilon_1/\varepsilon_2 = 1$. Bands of connected damage zones have developed at an angle of about 25° to the principal stress direction ε_2.

[1979, 1981]. *Ruina* [1983] and others interpreted results of laboratory friction experiments involving hold times of the pulling mechanism and jumps in sliding velocities in terms of rate- and state-dependent friction. As was mentioned in the introduction, the RS friction, like our model, provides a conceptual framework incorporating all important stages of an earthquake cycle. It is therefore useful to compare results based on our model predictions with laboratory measurements of RS frictional parameters.

In contrast to laboratory frictional experiments, our model does not have sliding surfaces, but rather damaged zones of weakness. Nevertheless, a comparison of our model results with laboratory RS (and other frictional) data is useful, since it allows us to adapt our model to macroscopic situations involving various faulting phenomena.

Following equation (20), material healing starts when the deformation is less than critical ($\xi<\xi_0$). As discussed in the context of Figure 3, for zero initial damage the coefficient ξ_0 may be estimated from the friction of the material. Once this coefficient is fixed, substituting the effective elastic moduli (13) into (37) we may calculate the friction angle as a function of the initial damage (Figure 9). This is not the same as the static friction that is measured in laboratory friction experiments, but both coefficients have a similar physical sense, and they are expected to be proportional to each other [*Savage et al.*, 1996].

Dieterich [1972] reported detailed results of frictional experiments with different normal stress and hold times up to 10^5 s and fitted the static friction with the equation

$$\mu_s = \mu^0 + A \log_{10}(1+Bt), \qquad (41)$$

where t is the duration of the hold time in seconds, $\mu^0\approx0.6$-0.8, $A\approx0.01$-0.02, and $B\approx1$-$2\ s^{-1}$. The results were interpreted as representing enlargement of the real contact area with time due to indentation creep around geometrical asperities. Using our previous assumption on the relation between α and μ_s and employing equation (20) for material healing under normal stress σ_n, the damage rheology model predicts linear increase of the static friction with time. This relation cannot fit the experimental data, and it leads to a quicker increase of μ_s than the logarithmic law. This suggests that the rate of healing depends on the damage itself. This imposes that for healing the damage rate coefficient is proportional to the exponent of the current level of α. Thus we substitute a function for the parameter C_d in equation (20) to incorporate different coefficients for degradation and healing in the form

$$\frac{d\alpha}{dt} = \begin{cases} C_d I_2(\xi-\xi_0) & \text{for } \xi \ge \xi_0 \\ C_1 \exp\left(\dfrac{\alpha}{C_2}\right) I_2(\xi-\xi_0) & \text{for } \xi \le \xi_0 . \end{cases} \qquad (42)$$

where C_d is constant describing the rate of degradation and C_1 and C_2 are constants describing the rate of healing. With this modification the equation for healing has the logarithmic solution

$$\alpha(t) = \alpha_0 - C_2 \ln(10) \times \log_{10}\left(1 - \frac{C_1}{C_2}\exp\left[\frac{\alpha_0}{C_2}\right] I_2(\xi-\xi_0)\, t\right). \qquad (43)$$

Thus a damage decrease (healing) starts from some initial value α_0 (Figure 10) which is critical value for any type of deformation ξ. Normal compression reduces the actual strain invariant ratio below ξ_0 and provides conditions for healing. According to (43), the healing is logarithmic in time in agreement with *Dieterich* [1972, 1979] and following works. Comparing (43) with equation (41) for static friction, and using the relation between damage and friction (Figure 9), we may suggest that the coefficient $C_2\ln(10)$ should be of the same order as A (i.e., $C_2\sim10^{-2}$), and the relation $C_1/C_2\exp\{[\alpha_0/C_2]I_2\}$ is of the same order as B.

Miao et al. [1995] reported experimental results showing time changes of Young's modulus during the healing of crushed rock salt. In those experiments, Young's modulus increases relatively fast at the beginning of the process. After 2000-3000 min the evolution rate significantly decreases, producing a logarithmic-like relationship between Young's modulus and densification time [*Miao et al.*, 1995, Figure 10]. Our model unifies this observed behavior with the experimental results of Dieterich on state dependent friction.

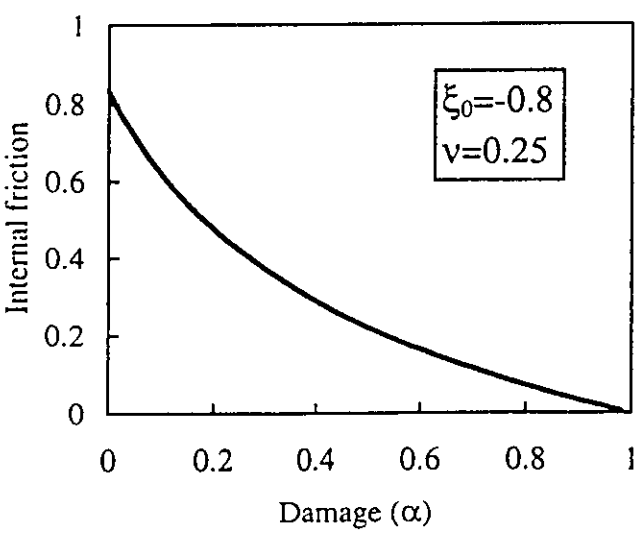

Figure 9. Variation of the friction as a function of damage α.

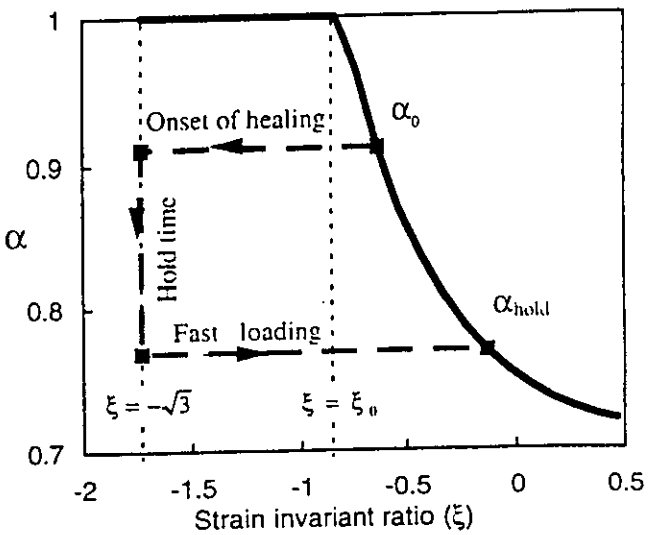

Figure 10. Material recovering in stationary contact from initial damage α_0 to α_{hold} due to normal stress. The increase of static friction is proportional to the logarithm of the hold time duration.

7. Discussion

We have described a damage rheology model based on thermodynamic principles and fundamental observations of rock deformation in situ and in the laboratory. The model has many realistic features of 3-D deformation fields which can be summarized as follows

7.1. Strength Degradation and Healing

A state of stress corresponding to strain $\xi>\xi_0$ leads to material degradation, with a rate proportional to the second strain invariant multiplied by $(\xi-\xi_0)$. Conversly, when $\xi<\xi_0$, the same process results in material strengthening. At each time the existing value of the damage parameter reflects an integrated history of the damage process. The values of the damage rate constants C_d and C_l in equation (42) define the duration of the rock memory for positive (degradation) and negative (healing) damage evolution, respectively. Infinitely large C_d and C_l correspond to zero memory, in which case the model gives ideal elastoplastic behavior. Infinitely small C_d and C_l give Hookean elastic behavior.

7.2. Process Zone

Positive damage evolution starts at low loading when the strain becomes critical ξ_0, and it produces gradual damage in a "process zone" around completely damaged ("destroyed") regions. Because of the finite size of the process zone, our model does not have the unphysical stress singularities of the ideal classical crack solution. The equations of stress have a regular solution at every point, and they incorporate fracture zones having a finite rate of growth. Such process zones are observed in many experiments with rocks and design materials [e.g., *Lockner et al.*, 1991] and their existence often governs the rate and trajectory of the failure evolution.

7.3. Aseismic Deformation, Strain Localization, and Seismic Events

When damage increases, values of the effective elastic moduli decrease, and at some point the elastic energy may lose its convexity. In that situation the slope of the stress-strain relation is negative. The strain localizes in a high damage zone with zero to negative effective moduli, and it may become unbounded if loading continues. The deformation preceding strain localization is stable or with negligible energy loss to seismic emission, while the deformation following strain localization is abrupt or seismic. Thus our model accounts for aseismic deformation, seismic events, and the transitions between these two modes of failure.

Simplified 1-D and 2-D versions of the damage rheology model lead to analytical results incorporating a variety of deformational phenomena, such as strain localization (equation 30) and stick-slip behavior (equation 36). A practical version of the general formulation provides a basic expression (equation 20) for the evolution of damage in terms of two model parameters: a critical deformation ξ_0 separating material degradation from healing, and a constant C_d governing the rate of damage evolution. We have attempted to constrain these parameters with relevant laboratory friction and acoustic emission data (Figures 4-8). Additional constraints are needed, especially for C_d. A variant of the basic damage evolution law, motivated by the time-dependent friction measurements of *Dieterich* [1972], contains two different forms (equation 42) for damage evolution during material degradation and healing. The modified evolution law provides logarithmic healing with time (equation 43) in agreement with the experimental results.

The damage rheology of the present work is used, together with additional developments, in a follow-up paper where we simulate the coupled evolution of regional earthquakes and faults. A number of potential improvements to our damage rheology model should be explored in parallel.

Acknowledgments. We thank J. Lister, Z. Reches, L. Slepyan for useful discussions, and A. Rubin, H. Schreyer, D. McTigue for constructive reviews. A. Agnon acknowledges support from the Binational Science Foundation, grant BSF-92344. V. Lyakhovsky was supported by the Golda Meir Foundation. Y. Ben-Zion was supported by the Southern California Earthquake Center (based on NSF cooperative agreement EAR-8920136 and USGS cooperative agreement 14-08-0001-A0899).

References

Agnon, A., and A. Eidelman, Lithospheric breakup in three dimensions: Necking of a work-hardening plastic plate, *J. Geophys. Res.*, *96*, 20,189-20,194, 1991.

Agnon, A., and V. Lyakhovsky, Damage distribution and localization during dyke intrusion, in The Physics and Chemistry of Dykes, edited by G. Baer and A. Heimann, pp. 65-78, A.A. Balkema, Brookfield, Vt., 1995.

Ambartsumyan, S.A., Raznomodulnaya Teoria Uprugosti (Strain-Dependence Elastic Theory), 320 pp., Nauka, Moscow, 1982.

Anderson, E.M., The Dynamics of Faulting, 183 pp., Oliver and Boyd, Edinburgh, Scotland, 1951.

Andrews, D. J., Rupture propagation with finite stress in antiplane strain, *J. Geophys. Res.*, *81*, 3575-3582, 1976.

Andrews, D. J., Mechanics of fault junctions, *J. Geophys. Res.*, *94*, 9389-9397, 1989.

Andrews, D. J., and Y. Ben-Zion, Wrinkle-like slip pulse on a fault between different materials, *J. Geophys. Res.*, *102*, 553-571, 1997.

Atkinson, B.K., and P.G. Meredith, The theory of subcritical crack growth with applications to minerals and rocks, in Fracture Mechanics of Rock, Academic, San Diego, Calif., edited by B.K. Atkinson, pp. 11-166, 1987.

Aviles, C.A., C.H. Scholz, and J. Boatwright, Fractal analysis applied to characteristic segments of the San Andreas fault, *J. Geophys. Res.*, *92*, 331-344, 1987.

Baer, G., Mechanisms of dike propagation in layered rocks and in massive, porous sedimentary rocks, *J. Geophys. Res.*, *96*, 11,911-11,929, 1991.

Barenblatt, G.I., The mathematical theory of equilibrium cracks in brittle fracture, in Advances in Applied Mechanics, pp. 55-129, Academic, San Diego, Calif., 1962.

Bazant, Z.P., and L. Cedolin, Stability of Structures, Elastic, Inelastic, Fracture and Damage Theories, 984 pp., Oxford Univ. Press, New York, 1991.

Ben-Avraham, Z., and V. Lyakhovsky, Faulting process along the northern Dead Sea transform and the Levant margin, *Geology*, *20*, 1143-1146, 1992.

Ben-Zion, Y., and J.R. Rice, Earthquake failure sequences along a cellular fault zone in a three-dimensional elastic solid containing asperity and nonasperity regions, *J. Geophys. Res.*, *98*, 14,109-14,131, 1993.

Ben-Zion, Y., and J.R. Rice, Slip patterns and earthquake populations along different classes of faults in elastic solids, *J. Geophys. Res.*, *100*, 12,959-12,983, 1995.

Brace, W.F., and D.L. Kohlstedt, Limits on lithospheric stress imposed by laboratory experiments, *J. Geophys. Res.*, *85*, 6248-6252, 1980.

Budiansky, B., and R.J. O'Connell, Elastic moduli of a cracked solid, *Int. J. Solids Struct.*, *12*, 81-97, 1976.

Burridge, R., and L. Knopoff, Model and theoretical seismicity, *Bull. Seismol. Soc. Am.*, *57*, 341-371, 1967.

Byerlee, J.D., Frictional characteristics of granite under high confining pressure, *J. Geophys. Res.*, 72, 3639-3648, 1967.

Carlson, J. M. and J. S. Langer. Mechanical model of an earthquake. *Phys. Rev. A. 40*. 6470-6484. 1989.

Chai, H.. Observation of deformation and damage at the tip of cracks in adhesive bonds loaded in shear and assessment of a criterion for fracture. *Int. J. Fract.. 60*. 311-326. 1993.

Chinnery, M.A.. Secondary faulting. 1. Theoretical aspects. Can. *J. Earth Sci.. 3*. 163-174. 1966.

Chinnery, M.A.. Secondary faulting. 2. Geological aspects. *Can. J. Earth Sci.. 3*. 175-190. 1966.

Chudnovsky, A.. W.-L. Huang and B. Kunin. Effect of damage on fatigue crack propagation in polystyrene. *Polym. Eng. Sci.. 30*. 1303-1308. 1990.

Coleman. B.D. and M.E. Gurtin. Thermodynamics with internal state variables. *J. Chem. Phys.. 47*. 597-613. 1967.

Cox. S.J.D.. and C.H. Scholz. Rupture initiation in shear fracture of rocks: an experimental study. *J. Geophys. Res.. 93*. 3307-3320. 1988.

Cowie. P.. C. Vanneste. and D. Sornette. Statistical physics model for the spatio-temporal evolution of faults. *J. Geophys. Res.. 98*. 21.809-21.821. 1993.

deGroot. S.R.. and P. Mazur. *Nonequilibrium Thermodynamics*. 510 pp.. North-Holland New York. 1962.

Delaney. P.T.. D.D. Pollard. J.I. Ziony. and E.H. McKee. Field relations between dikes and joints: Emplacement processes and paleostress analysis. *J. Geophys. Res.. 91*. 4920-4938. 1986.

Dieterich. J.H.. Time-dependent friction in rocks. *J. Geophys. Res.. 77*. 3690-3697. 1972.

Dieterich. J. H.. Modeling of rock friction. 1. Experimental results and constitutive equations. *J. Geophys. Res.. 84*. 2161-2168. 1979.

Dieterich. J. H.. Constitutive properties of faults with simulated gouge. in *Mechanical Behavior of Crustal Rocks: The Handin Volume. Geophys. Monogr. Ser.*. vol. 24. pp. 103-120. AGU. Washington. D.C.. 1981.

Dugdale. D.S.. Yielding of steel sheets containing slits. *J. Mech. Phys. Solids. 8*. 100-104. 1960.

Ekland. I.. and R. Temam. *Convex Analysis and Variational Problems*. 390 pp.. Elsevier. New York. 1976.

Fitts. D.D.. *Nonequilibrium Thermodynamics*. 173 pp.. McGraw-Hill. New York. 1962.

Freund. L.B.. *Dynamic Fracture Mechanics*. 563 pp.. Cambridge Univ. Press. New York. 1990.

Gibbs. J.W.. *The Scientific Papers*. vol. 1. *Thermodynamics*. New York. 1961.

Hansen. N.R.. and H.L. Schreyer. A thermodynamically consistent framework for theories of elastoplasticity coupled with damage. *Int. J. Solids Struct.. 31*. 359-389. 1994.

Hansen. N.R.. and H.L. Schreyer. Damage deactivation. *J. Appl. Mech.. 62*. 450-458. 1995.

Hoek. J.D.. Dyke propagation and arrest in Proterozoic tholeiitic dyke swarms. Vestfold Hills. East Antarctica. in *The Physics and Chemistry of Dykes*. edited by G. Baer and A. Heimann. pp. 79-95. A.A. Balkema. Brookfield. Vt.. 1995.

Hoff. N.J.. The necking and rupture of rods subjected to constant tensile loads. *J. Appl. Mech.. 20*. 105-108. 1953.

Huang. W.-L.. B. Kunin. and A. Chudnovsky. Kinematics of damage zone accompanying curved crack. *Int. J. Fract.. 50*. 143-152. 1991.

Hull. J.. Thickness-displacement relationships for deformation zones. *J. Struct. Geol.. 10*. 431-435. 1988.

Ida. Y.. Cohesive force across the tip of longitudinal shear crack and Griffith's specific surface energy. *J. Geophys. Res.. 77*. 3796-3805. 1972.

Irwin. G.R.. Elasticity and Plasticity. in Handbuch der Physik. vol. VI edited by S. Flugge. pp. 551-590. Springer. Berlin. 1958.

Jones. R.M.. Stress-stain relation for materials with different moduli in tension and compression. *AIAA J.. 15*. 62-73. 1977.

Ju. J.W.. Isotropic and anisotropic damage variables in continuum damage mechanics. *J. Eng. Mech.. 116*. 2764-2770. 1990.

Kachanov. L.M.. On the time to rupture under creep condition (in Russian). *Izv. Acad. Nauk SSSR. Otd. Tekh. Nauk. 8*. 26-31. 1958.

Kachanov. L.M.. *Introduction to Continuum Damage Mechanics*. 135 pp.. Martinus Nijhoff. Dordrecht. Netherlands. 1986.

Kachanov. M.. Elastic solids with many cracks and related problems. in *Advances in Applied Mechanics*. vol. 30. edited by J. Hutchinson and T. Wu. pp. 259-445. Academic Press. 1993.

Kachanov. M.. On the concept of damage in creep and in the brittle-elastic range. *Int. J. Damage Mech.. 3*. 329-337. 1994.

King. G.. The accommodation of large strains in the upper lithosphere of the Earth and other solids by self-similar fault systems: The geometrical origin of b-value. *Pure Appl. Geophys.. 121*. 761-814. 1983.

Lockner. D.A. and J.D. Byerlee. Development of fracture planes during creep in granite. in *2nd Conference on Acoustic Emission/Microseismic Activity in Geological Structures and Materials*. pp. 1-25. Trans Tech.. Clausthal-Zellerfeld. Germany. 1980.

Lockner. D.A.. and T.R. Madden. A multiple-crack model of brittle fracture. 1. Non-time-dependent simulation. *J. Geophys. Res. 96*. 19.623-19.642. 1991a.

Lockner. D.A.. and T.R. Madden. A multiple-crack model of brittle fracture. 1. Non-time-dependent simulation: 2. Time-dependent simulation. *J. Geophys. Res. 96*. 19.643-19.654. 1991b.

Lockner. D.A.. J.D. Byerlee. V. Kuksenko. A. Ponomarev. and A. Sidorin. Quasi-static fault growth and shear fracture energy in granite. *Nature. 350*. 39-42. 1991.

Lomakin. E.V.. and Yu.N. Rabotnov. Sootnosheniya teorii uprugosti dlya isotropnogo raznomodulnogo tela (Constitutive relationships for the strain-dependent elastic body). *Izv. Akad. Nauk SSSR Mekh. Tverd. Tela. 6*. 29-34. 1978.

Lubliner. J.. On the thermodynamic foundations of nonlinear solids mechanics. *Int. J. Nonlinear Mech.. 7*. 237-254. 1972.

Lyakhovsky. V.. The effective viscosity of a microfractured medium. (in Russian) no. 4. 94-98. 1988. (English translation. *Izv. Acad. Sci. USSR Phys. Solid Earth*. Engl. Transl.. *24*(4). 318-320. 1988.)

Lyakhovsky. V.A.. Application of the multimodulus model to analysis of stress-strain state of rocks. (in Russian) no 2. 89-94. 1990. (English translation. *Izv. Acad. Sci. USSR Phys. Solid Earth*. Engl. Transl.. 26(2). 177-180. 1990.)

Lyakhovsky. V.A.. and V.P. Myasnikov. On the behavior of elastic media with microdisturbances. (in Russian) no 10. 71-75. 1984. (English translation. *Izv. Acad. Sci. USSR Phys. Solid Earth*. Engl. Transl.. 20(10). 769-772. 1984.)

Lyakhovsky. V.A.. and V.P. Myasnikov. On the behavior of viscoelastic medium with microfractures subjected to extension and shear. (in Russian) no 4. 28-35. 1985. (English translation. *Izv. Acad. Sci. USSR Phys. Solid Earth*. Engl. Transl.. 21(4). 265-270. 1985.)

Lyakhovsky. V.A.. and V.P. Myasnikov. Relation between seismic wave velocity and state of stress. *Geophys. J. R. Astron. Soc.. 2*. 429-437. 1987.

Lyakhovsky. V.A.. and V.P. Myasnikov. Acoustics of rheologically nonlinear solids. *Phys. Earth Planet. Inter.. 50*. 60-64. 1988.

Lyakhovsky. V.. Y. Podladchikov. and A. Poliakov. Rheological model of a fractured solid. *Tectonophysics. 226*. 187-198. 1993.

Lyakhovsky. V.. Z. Ben-Avraham. and M. Achmon. The origin of the Dead Sea rift. *Tectonophysics. 240*. 29-43. 1994.

Lyakhovsky. V.. Z. Reches. R. Weinberger. and T.E. Scott. Nonlinear elastic behavior of damaged rocks. *Geophys. J. Int.. 130*. 157-166. 1997.

Malvern. L.E.. *Introduction to the Mechanics of a Continuum Medium*. 713 pp.. Prentice-Hall. Englewood Cliffs. N. J.. 1969.

Miao. S.. M.L. Wang. and H.L. Schreyer. Constitutive models for healing of materials with application to compaction of crushed rock salt. *J. Appl. Mech.. 62*. 450-458. 1995.

Mosolov. P.P.. and V.P. Myasnikov. Variational methods in flow theory of visco-plastic media. (in Russian). *Prikl. Math. Mekh.. 29*. 468-492. 1965.

Myasnikov. V.P.. V.A. Lyakhovsky. and Yu.Yu. Podladchikov. Nonlocal model of strain-dependent visco-elastic media. (in Russian). *Dokl. Acad. Sci. USSR. 312*. 302-305. 1990.

Nishihara. M.. Stress-strain relation of rocks. *Doshisha Eng. Rev.. 8*. 32-54. 1957.

Onsager. L.. Reciprocal relations in irreversible processes. *Phys. Rev.. 37*. 405-416. 1931.

Okubo. P.G.. and K. Aki. Fractal geometry in the San Andreas fault system. *J. Geophys. Res.. 92*. 345-355. 1987.

Palmer. A. C.. and J. R. Rice. The growth of slip surfaces in the progressive failure of over-consolidated clay. *Proc. R. Soc. London. Ser. A. 332*. 527-548. 1973.

Papa, E., A damage model for concrete subjected to fatigue loading, *Eur. J. Mech. A Solids, 12*, 429-440, 1993.

Papageorgiou, A. S., and K. Aki, A specific barrier model for the quantitative description of inhomogeneous faulting and the prediction of strong ground motion, II, Applications of the model, *Bull. Seismol. Soc. Am., 73*, 953-978, 1983.

Prigogine, I., *Introduction to Thermodynamics of Irreversible Processes*, 115 pp., Thomas, Springfield, Illinois, 1955.

Rabotnov, Y.N., *Creep Problems in Structural Members*, 822 pp., North-Holland, Amsterdam, 1969.

Rabotnov, Y.N., *Mechanics of Deformable Solids*, (in Russian), 712 pp., Science, Moscow, 1988.

Rabinovicz, E., *Friction and Wear of Materials*, pp. 97-99, John Wiley, New York, 1965.

Reches, Z., Faulting of rocks in three-dimensional strain fields, II, Theoretical analysis, *Tectonophysics, 95*, 133-156, 1983.

Reches, Z., Evolution of fault patterns in clay experiments, *Tectonophysics, 145*, 141-156, 1988.

Reches, Z., and D.A. Lockner, Nucleation and growth of faults in brittle rocks, *J. Geophys. Res., 99*, 18,159-18,173, 1994.

Rice, J. R., Spatio-temporal complexity of slip on a fault, *J. Geophys. Res., 98*, 9885- 9907, 1993.

Rubin, A.M., Propagation of magma filled cracks, *Anu. Rev. Earth Planet. Sci. 8*, 287-336, 1995a.

Rubin, A.M., Why geologists should avoid using "fracture toughness" (at least for dikes), in *The Physics and Chemistry of Dykes*, edited by G. Baer and A. Heimann, pp. 53-65, A.A. Balkema, Brookfield, Vt., 1995 b.

Rudnicki, J.W., and J.R. Rice, Conditions for the localization of deformation in pressure-sensitive, dilatant materials, *J. Mech. Phys. Solids, 23*, 371-394, 1975.

Ruina, A., Slip instability and state variable friction laws, *J. Geophys. Res., 88*, 10,359- 10,370, 1983.

Robertson, E.C., Relationship of fault displacement to gouge and breccia thickness, *Min. Eng., 35*, 1426-1432, 1983.

Robinson, E.L., Effect of temperature variation on the long-term rupture strength of steels, *Trans. ASME, 174*, 777-781, 1952.

Sammonds, P.R., P.G. Meredith, and I.G. Main, Role of pore fluids in the generation of seismic precursors to shear fracture, *Nature, 359*, 228-230, 1992.

Savage, J.C., J.D. Byerlee, and D.A. Lockner, Is internal friction friction?, *Geophys. Res. Lett., 23*, 487-490, 1996.

Scholz, C.H., *The Mechanics of Earthquakes and Faulting*, 439 pp., Cambridge Univ. Press, New York, 1990.

Schreyer, H.L., and M.K. Neilsen, Analytical and numerical tests for loss of material stability, *Int. J. Num. Methods Eng., 39*, 1721-1736, 1996.

Schreyer, H.L., and M.K. Neilsen, Discontinuous bifurcation states for associated smooth plasticity and damage with isotropic elasticity, *Int. J. Solids Struct., 33*, 3239-3256, 1996b.

Sedov, L.I., Variational methods of constructing models of continuos media, in *Irreversible Aspects of Continuum Mechanics*, pp. 17-40 Springer-Verlag, New York, 1968.

Segall, P., and D.D. Pollard, Nucleation and growth of strike slip faults in granite, *J. Geophys. Res., 88*, 555-568, 1983.

Sornette, D., P. Miltenberger, and C. Vanneste, Statistical physics of fault patterns self-organized by repeated earthquakes, *Pure Appl. Geophys., 142*, 491-527, 1994.

Stesky, R.M., W.F. Brace, D.K. Riley, and P.Y.F. Robin, Friction in faulted rock at high temperature and pressure, *Tectonophysics, 23*, 177-203, 1974.

Storen, S., and J.R. Rice, Localized necking in thin sheets, *J. Mech. Phys. Solids, 23*, 421-441, 1975.

Swanson, P.L., Subcritical crack growth and other time and environment-dependent behavior in crustal rocks, *J. Geophys. Res., 89*, 4137-4152, 1984.

Turcotte, D.L., Fractals and fragmentation, *J. Geophys. Res., 91*, 1921-1926, 1986.

Valanis, K.C, A theory of damage in brittle materials, *Eng. Fract. Mech., 36*, 403-416, 1990.

Walsh, J.B., The effect of cracks on the uniaxial elastic compression of rocks, *J. Geophys. Res., 70*, 399-411, 1965.

Ward, S.N., A synthetic seismicity model for Southern California: Cycles, probabilities, and hazard, *J. Geophys. Res., 101*, 22,393-22,418, 1996.

Weinberger, R., Z. Reches, T.S. Scott, and A. Eidelman, Tensile properties of rocks in four-point beam tests under confining pressure, pp. 435-442, in Proceedings First North American Rock Mechanics Symposium, Austin, Tex., 1994.

Weinberger, R., G. Baer, G. Shamir, and A. Agnon, Deformation bands associated with dyke propagation in porous sandstone, Makhtesh Ramon, Israel, in The Physics and Chemistry of Dykes, edited by G. Baer and A. Heimann, pp. 95-115, A.A. Balkema, Brookfield, Vt., 1995.

Yukutake, H., Fracturing process of granite inferred from measurements of spatial and temporal variations in velocity during triaxial deformation, *J. Geophys. Res., 94*, 15,639-15,651, 1989.

A. Agnon and V. Lyakhovsky, Institute of Earth Sciences, The Hebrew University, Givat Ram, Jerusalem, 91904 Israel. (e-mail: vladi@cc.huji.ac.il.)

Y. Ben-Zion, Department of Earth Sciences, University of Southern California, Los Angeles, CA 90089-0740. (e-mail: benzion@terra.usc.edu)

(Received October 29, 1996; revised June 4, 1997;
accepted June 30, 1997.)